Surface photochemistry in the vacuum and extreme ultraviolet (VUV and XUV): high harmonic generation, H_2O and O_2

2006 J. Phys.: Condens. Matter 18 S1655

(http://iopscience.iop.org/0953-8984/18/30/S14)

INSTITUTE OF PHYSICS PUBLISHING JOURNAL OF PHYSICS: CONDENSED MATTER

J. Phys.: Condens. Matter **18** (2006) S1655–S1675 doi:10.1088/0953-8984/18/30/S14

Surface photochemistry in the vacuum and extreme ultraviolet (VUV and XUV): high harmonic generation, H_2O and O_2

Kurt W Kolasinski

Department of Chemistry, University of Virginia, PO Box 400319, McCormick Road, Charlottesville, VA 22904-4319, USA

E-mail: Kolasinski@virginia.edu

Received 27 September 2005, in final form 27 October 2005
Published 14 July 2006
Online at stacks.iop.org/JPhysCM/18/S1655

Abstract

Techniques to produce light in the vacuum ultraviolet (VUV; 100 nm $\leqslant \lambda \leqslant$ 200 nm) and extreme ultraviolet (XUV; 10 nm $\leqslant \lambda \leqslant$ 100 nm) are reviewed. Special emphasis is placed on high harmonic generation (HHG). Experimental studies that have utilized HHG as well as the VUV and XUV surface photochemistry of H_2O and O_2 are reviewed. HHG is shown to be a promising technique for the investigation of the dynamics of electrons and surface photochemistry. Lateral interactions and adsorbate structure in adsorbed H_2O and O_2 layers are shown to have important roles in determining the fate of ions produced by dissociative photoionization at surfaces.

1. Introduction

This article concerns itself with surface photochemistry in the VUV and XUV spectral ranges as well as the techniques used to generate this light. Here we define three regions: the ultraviolet (UV; 200 nm $\leqslant \lambda \leqslant$ 400 nm, 3.1–6.2 eV), vacuum ultraviolet (VUV; 100 nm $\leqslant \lambda \leqslant$ 200 nm, 6.2–12.4 eV) and extreme ultraviolet (XUV; 10 nm $\leqslant \lambda \leqslant$ 100 nm, 12.4–124 eV). The VUV and XUV are particularly active regions for photochemistry because the transitions of valence electrons—the electrons most directly involved in chemical bonding—lie in these regions. However, several materials' properties conspire to complicate the study of surface photochemical phenomena in this region. The first is what is responsible for the vacuum of the vacuum ultraviolet. Atmospheric absorption, first by oxygen and then by nitrogen, greatly limits the pathlength of electromagnetic radiation below 200 nm. Anyone who has been near a 100 Hz (or greater) repetition rate ArF excimer laser operating at 193 nm will know the smell of photochemically produced ozone. The pathlength of the only other commercial VUV laser, the fluorine laser operating at 157 nm, has a pathlength too short to make for practical use under ambient conditions. The second materials' problem is that VUV and XUV radiation interact

strongly with solid materials [1]. Metals are no longer highly reflective, necessitating the use of specially designed multilayer mirrors [2]. The very best quartz cannot be used as an optical material below 175 nm. CaF_2 extends to 125 nm for use as a window and MgF_2 to 122 nm. The highest band gap material, LiF, can be used as a window down to 104.5 nm.

The third materials' problem is related to the lasing medium. Several schemes exist for producing tunable UV radiation including lasers that operate directly in this region as well as nonlinear optical techniques (harmonic generation, parametric generation, etc). Broadly tunable sources operating in the VUV and XUV are a much rarer commodity. This can be traced back to quantum mechanical fundamentals as revealed by the ratio of the Einstein coefficients for spontaneous and stimulated emission between two levels. At progressively higher frequencies, the rate of spontaneous emission becomes increasingly larger than that for stimulated emission. Therefore, for energy levels separated by increasingly larger gaps and shorter lifetimes, it becomes progressively more difficult to maintain the population inversion required for lasing.

Compared with conventional studies of surface photodynamics in the visible and near UV, the VUV has two principal attractions:

(i) it is a region where many simple molecules with well-characterized gas-phase photochemistry and thermal surface chemistry (e.g. O_2, CO, H_2O) absorb light; and
(ii) the photon energy exceeds the work function of the substrate, allowing the generation of substrate photoelectrons which can drive dynamical processes in an adsorbed molecular film.

Surface photochemistry in the VUV and XUV is of particular importance to the evolution of the interstellar medium, protoplanetary clouds [3, 4] and elsewhere in our solar system [5] as well as to semiconductor processing [6–10]. The extension of top-down lithographic techniques to the patterning of self-assembled monolayers represents a potentially powerful route to not only surface but also three-dimensional nanoarchitectures [11]. Because a range of different molecular electronic states exist at these energies, VUV photons can excite surface photochemistry that can exhibit specific resonant behaviour [12, 13] and that can be compared to gas-phase photochemistry in the VUV [14]. Recently, the first experiments in which VUV light generated by high harmonic generation (HHG) was used to excite [15] and to probe [16, 17] surface photochemistry were reported. This review will place special emphasis on HHG as well as the photochemistry of two important small molecules, O_2 and H_2O.

2. VUV and XUV light sources

2.1. Atomic lamps

One of oldest sources of VUV and XUV light is atomic emission lamps excited by any of a variety of discharges [1]. Of particular interest for astrochemical studies are the emission lines of H (10.2 eV), and He (21.1 and 40.82 eV) because these are the most abundant species in the interstellar medium. They also deliver some of the highest intensity short wavelength radiation and commercial sources can now deliver of the order of 10^{13} photons cm^{-2} s^{-1}. Different rare gases can be used to deliver other photon energies. These sources are continuous wave, i.e. not pulsed, sources that require windowless operation; hence, they affect the pressure in the surface science chamber. Furthermore, useful photon fluxes are, for most purposes, only available at discrete lines since the continuum radiation between these lines tends to be produced at much lower intensity. Xe flash lamps can be operated to provide μs pulses of light in the range 170–3000 nm, with time-averaged powers exceeding 100 mW.

2.2. Synchrotrons

Accelerating electrons emit radiation. The recognition of this was a primary objection to the planetary model of negatively charged electrons orbiting a positive nucleus and led Bohr to his ad hoc proposition for the quantization of angular momentum. This parasitic phenomenon was originally observed as a complication in the construction and operation of high-energy electron accelerators but then it was soon realized that this could be exploited as a light source [2]. Thus was born the synchrotron, and the first implementation was at General Electric in 1947 [2]. A recent survey of synchrotron facilities is available from the proceedings of the 8th International Conference on Synchrotron Radiation Instrumentation [18]. Third generation synchrotron sources operate continuously between 10–1000 eV (and beyond). They can deliver up to 10^{13} photons s^{-1} into a bandwidth of 0.01%. Different types of pulse trains are possible but typically high repetition rates (1–500 MHz) lead to low pulse energies in ∼100 ps pulses [19]. Therefore they are ideal for applications that require high average photon fluxes of incoherent radiation but they generally cannot reach the high power densities required to study nonlinear phenomena. Fourth generation sources, incorporating energy recoverable linacs (ERLs) and free electron lasers, promise to push pulse length into the sub-picosecond regime [18].

2.3. Free electron lasers

A free electron laser (FEL) consists of an electron beam propagating through a periodic magnetic field [20–22]. This transverse oscillating magnetic field is known as the undulator. Lasing occurs because the wiggler and the radiation combine to produce a beat wave that is synchronized with the electrons. An FEL is continuously tunable, capable of high peak and average powers, and can produce a range of pulse widths and patterns.

The Jefferson Laboratory FEL is a sub-picosecond (∼100 fs), tunable light source covering the range from 250 nm in the ultraviolet to 14 μm in the mid-infrared, with pulse energies up to 300 μJ, and at repetition rates up to 75 MHz. Not all parameters can be satisfied simultaneously but average powers in excess of 10 kW have been demonstrated in the infrared [21]. Because of the high peak power, the wavelength range could potentially be extended by conventional and high harmonic generation. The major advantage of an FEL over a synchrotron is that it can produce coherent light many orders of magnitude brighter than the incoherent synchrotron radiation [21].

The Deutsches Elektronen-Synchrotron (DESY) Laboratory is also planning an x-ray FEL. The FEL has operated in the range 80–180 nm since 2002. This has recently been extended to 6 nm and plans exist to reach an ultimate wavelength of just below 0.1 nm. An initial set of experiments at 98 nm has looked at the damage caused by the irradiation of Si, SiO_2, Au, PMMA and thin Au and C coatings on Si wafers with fluences up to >1 J cm^{-2} [22]. Photodesorbed ions with high translational energies were observed to leave the samples for high fluence irradiation. Ion desorption generally exhibited a threshold of 50 mJ cm^{-2}.

As of 2000, there were five FELs that could operate below 300 nm. Operation below 200 nm is severely limited by the poor quality of mirrors [20], which necessitates the use of a single pass self amplified spontaneous emission (SAES) scheme or high-gain harmonic generation (HGHG). HGHG requires a first, short undulator, called the modulator, to be tuned to the frequency of the coherent seed laser, which may be a short pulse optical laser. The second undulator, called the radiator, is tuned to the nth harmonic of the seed frequency. This scheme may facilitate the generation of XUV light with pulse lengths approaching 10 fs. Other schemes have been discussed with the intention of dropping the pulse length to as low as 200 as [22].

2.4. $\chi^{(3)}$ methods

Methods for generating VUV radiation via the third order nonlinear susceptibility have been reviewed by Lipson *et al* [19]. For laser intensities that are not too intense, the polarization $\boldsymbol{P}(\omega)$ induced in an irradiated material can be written as a Taylor series of the external electric field $\boldsymbol{E}(\omega)$

$$\boldsymbol{P}(\omega) = N(\chi^{(1)} \cdot \boldsymbol{E}(\omega) + \chi^{(2)} : \boldsymbol{E}(\omega)\boldsymbol{E}(\omega) + \chi^{(3)} : \boldsymbol{E}(\omega)\boldsymbol{E}(\omega)\boldsymbol{E}(\omega) + K) \tag{1}$$

where N, $\chi^{(1)}$ and $\chi^{(n)}$, $n \geqslant 2$, are the number density, linear susceptibility, and the nth order nonlinear susceptibility tensors of the medium, respectively. The real component of the $\chi^{(1)}$ term (refractive index) is responsible for the linear dispersive properties of the material, while its imaginary component describes absorption. Each higher order term in $\boldsymbol{E}(\omega)$ acts as a source for coherent light at new frequencies.

The $\chi^{(2)}$ term is responsible for second order phenomena such as second harmonic generation (SHG) and optical parametric oscillation. β-barium borate was greeted as a *Wunderkind* of nonlinear optical crystals when it burst onto the scene in the mid-1980s. This high damage threshold, widely transparent material with a $\chi^{(2)}$ value >4 times that of the old standard potassium dihydrogen phosphate (KDP) facilitated expanded studies in the UV. For example, the $(2+1)$ resonance enhanced multiphoton ionization scheme for H_2 through the E, F $^1\Sigma_g^+$ state was transformed from an arduous task involving fourth order anti-Stokes Raman shifting to produce several μJ per pulse [23, 24], to a straightforward tripling scheme producing >1 mJ per pulse. This greatly enhanced the detection sensitivity for H_2 and its isotopomers and ushered in an era of state-resolved surface studies [25–29].

However, BBO and all other nonlinear crystals are opaque below 189 nm, and hence, to most of the VUV and XUV. Consequently, VUV and XUV generation must be done in gaseous media, for which harmonic generation is dependent on the third order $\chi^{(3)}$ term. Two approaches to the production of VUV radiation in gaseous media are nonresonant tripling (third harmonic generation, THG) and two-photon resonance enhanced four-wave mixing. These techniques can be used to access the region 66–200 nm ($\sim$6–19 eV) with laser-like emission. However, gaps exist and the emission intensity varies significantly across this region. Peak intensities of 10^{12} photons s^{-1} are possible in 10 ns pulses with very narrow bandwidth ($\sim$0.5 cm^{-1}) [19]. The nonlinear medium is contained either in a heat pipe or static gas cell (limited in wavelength range by the windows) or in a supersonic gas jet expansion.

Whereas alkali metal vapours were first used as the tripling media, rare gases (Ne, Ar, Kr and Xe) as well as Hg are now more commonly used. Rare gases possess the distinct advantages that they are much easier to handle, and can be utilized either in a static gas cell or after expansion in a supersonic jet. Jets offer a virtually ideal 'windowless' environment for VUV generation. Conversion efficiencies of 10^{-8}–10^{-5} are possible using commercial nanosecond pulsed dye lasers with peak powers of 1–10 MW [19].

Hodgson *et al* [30] demonstrated that compared to THG substantially higher intensities and broader tunability in the VUV could be had with four-wave mixing in Sr vapour. Four-wave mixing is a variation on THG that requires two lasers. A VUV or XUV photon can be generated when three input fundamental photons from two lasers, two at frequency ω_1, and the other at frequency ω_2, are used to produce a fourth output photon at either the sum $(2\omega_1 + \omega_2)$ and/or the difference $(2\omega_1 - \omega_2)$ frequency. Resonance enhancement of the intensity occurs when one or more of the frequencies involved is coincident with a real electronic level in the atomic medium. The most common condition is that $2\omega_1$ is chosen to be resonant.

2.5. Plasma sources

Plasma sources operating around 13.5 nm are being considered as the basis of extreme ultraviolet (EUV) lithography [7], which is scheduled for commercial implementation in 2009 [10]. It should be noted that the progress of optical lithography has far exceeded the wildest imagination of process designers [31] and whereas it was once envisioned that EUV would be required at the 100 nm critical dimension node of integrated circuit fabrication [8, 32], its introduction is now planned for the 32 nm node [33]. The principles and methods of performing lithography with soft x-rays at ∼1 nm have been thoroughly reviewed by Turcu and Dance [34] and many of the same issues face EUV lithography. These authors also discuss short wavelength microscopy. Two competing technologies, gas discharge-produced plasma (GDPP) and laser-produced plasma (LPP), are vying to form the basis of a commercial lithography instrument and supply the estimated 115 W of useful incoherent optical power at a 7–10 kHz repetition rate that is required for economical illumination of silicon wafers. Such sources are being designed with maximum throughput and longevity in mind and are not intended to be tunable. The choice of wavelength has largely been chosen to coincide with the short wavelength limit of the reflectivity of Mo/Si multilayer mirrors [9].

Plasma sources [9, 10, 34] rely on either the blackbody emission of a Xe or Sn plasma at a temperature of 22 000 K to produce light at 13.5 nm or else from line emission of Li. Sn and Li are chosen because they are the most efficient emitters in the spectral region around 13.5 nm. Xe is chosen because of its ease of handling and lack of contamination risk, even though its spectrum peaks around 11 nm. The GDPP EUV source uses the Z-pinch principle to form a discharge in either Xe or Sn. In this type of discharge a magnetic field is used to compress a cold, low-density plasma into a sufficiently hot and high-density plasma. The discharge requires 20 kA of current and a magnetic field of 20 T is used to produce a 2000 bar plasma pressure. These sources presently can run at repetition rates in excess of 1 kHz and deliver >40 W of useful power. Since it is better matched to the sought-after 13.5 nm wavelength, Sn offers higher conversion efficiencies of pump power into light than does Xe.

LPP sources [32] offer some advantages regarding thermal management and compactness. They consist of a Xe or Sn jet as a target that is pumped by, for instance, a 1200 W 10 kHz Nd:YAG laser [10] providing a fluence of 10^{11}–10^{12} W cm^{-2}. Up to 10 W of useful 13.5 nm light is expected to be achieved with these pump lasers. Whereas earlier sources involved the irradiation of solid targets or atomic or cluster beams, the most recent devices use targets composed of droplets or solid filaments formed by a liquid jet. Scaling of LPP sources to commercially useful powers will require an order of magnitude increase in the pump laser power. For both GDPP and LPP, the mitigation of debris from electrodes and targets is crucial to producing a source with a lifetime in excess of 30 000 h, which corresponds to hundreds of millions of shots.

2.6. X-ray lasers

Lasers that operate in the VUV and XUV regions [35], excluding the ArF and F_2 excimer lasers, are commonly called x-ray lasers. In this context an x-ray laser is a laser that operates below 157 nm on the basis of a more or less conventional extension of the principles of IR, visible and UV lasers. That is, an (ionized) atomic medium is pumped to produce a population inversion, which leads to amplified stimulated emission. These lasers offer a high photon yield and peak power but suffer from limited tunability. They are conventionally pumped either by extremely powerful lasers (approaching 1 J/pulse) or electrical discharges with currents approaching 100 kA in a pulsewidth of a few tens of nanoseconds to produce highly ionized plasmas.

The technical difficulties associated with short excited state lifetimes, high pump power and low reflectivity of materials made realization of lasers in the XUV an imposing task. Nevertheless, significant amplification in this regime was achieved in 1984, when Matthews *et al* [36, 37] at $\lambda \approx 20$ nm and Suckewer *et al* [38] at $\lambda \approx 18$ nm, observed amplification from the generation of population inversions in plasmas. However, the complexity, cost, size and low repetition rates of these lasers still pose barriers to more common implementation.

One system pumped by an electrical discharge produced an average pulse energy of 0.88 mJ at 46.9 nm and a repetition rate of 4 Hz. The pulse width is around a nanosecond [39]. A 70 mJ, 40 fs, 10 Hz Ti:sapphire laser has been used to pump emission in the 30–50 nm range by creating a plasma of Pd-like Xe [40]. Such systems may be able to reach pulse energies of 1–10 μJ. Other pumping schemes involve the use of megalasers such as the petawatt lasers found in the National Ignition Facility at Lawrence Livermore National Laboratory [41] and the Vulcan program at the Rutherford Laboratory [42].

Zeitoun *et al* [43] have used light produced by high harmonic generation as a seed beam for an x-ray laser. The seed beam is introduced into a plasma amplifier pumped by a 1 J, 30 fs infrared pulse. The seed pulse is created with a 20 mJ, 30 fs infrared pulse.

2.7. High harmonic generation

Depending on ever-higher order terms in equation (1) to deliver progressively higher harmonics of the fundamental radiation is a losing battle. Each successive $\chi^{(n)}$ term is orders of magnitude weaker than the previous term. This necessitates the use of progressively higher laser intensities to achieve significant intensity in the succeeding harmonics. Eventually the laser intensity will become so great that the perturbation theory based expansion of equation (1) is no longer valid.

A two-step, semiclassical model is most often used to describe high harmonic generation (HHG) [44], though there are indications that a direct interaction between free electrons and the optical field may make a contribution to the process as well [45]. As the laser fluence approaches and exceeds 10^{13} W cm^{-2}, the electric field of the optical field approaches the strength of the Coulomb potential that holds the electrons in an atom or molecule and actually suppresses this barrier during the first half cycle of the optical pulse. This regime is routinely accessible with commercially available Ti:sapphire lasers. An electron tunnels out of the atom and finds itself with zero kinetic energy. Most of the electrons simply detach from the ion core, resulting in photoionization. During the second half cycle of the optical pulse in which the electric field has then changed sign, some of the electrons will be accelerated back into the ion core. The acceleration is quantized as energy can only be taken out of the optical field in units of the photon energy of the fundamental radiation. When the electron recombines with the ion core, the energy gained in this process is lost as radiation. For a spherically symmetric medium such as an atom, symmetry constraints (parity conservation) demand that only odd harmonics are generated. This restriction is relaxed in molecular media [46–49], though they exhibit other characteristics (e.g. low ionization potential, extensive dissociation) that tend to limit the conversion efficiency.

In an alternative fully quantal model, electrons are injected into the optical field by above threshold ionization (ATI). They then interact with photons to form stationary Volkov states and the HHG spectrum results from transitions between these states. The stationary nature of the Volkov states, which can be regarded as the high optical field analogue of the bound states of an atom, ensures that the total energy and momentum of the electron–photon system are well defined and that the resulting HHG photons are produced at well-defined energies corresponding to odd harmonics of the fundamental photon frequency.

Either of these coherent nonlinear processes makes possible the generation of photons with energies exceeding 500 eV [50–53] with sub-femtosecond pulse widths (1 fs $= 1 \times 10^{-15}$ s).

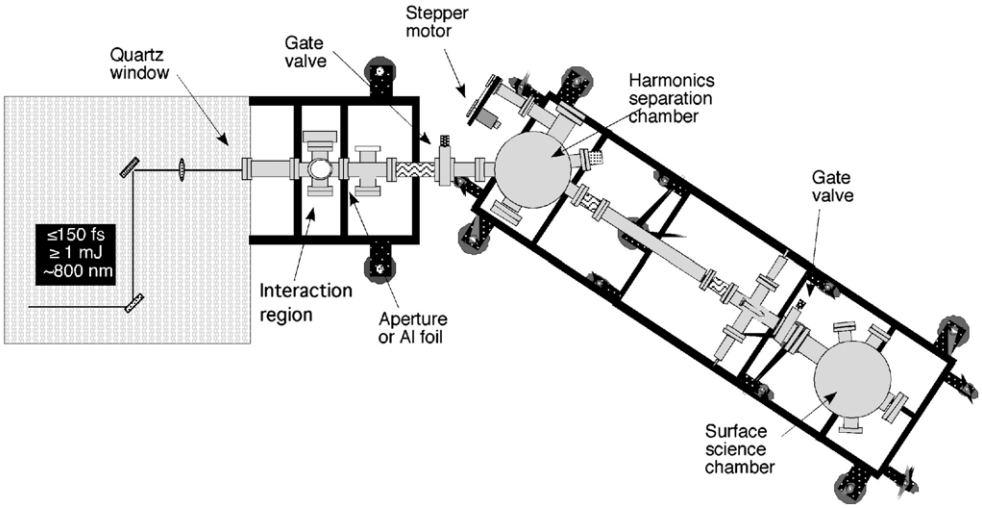

Figure 1. Schematic diagram of a typical optical/vacuum system used to implement HHG in surface science studies.

The realm of attosecond (1 as $= 1 \times 10^{-18}$ s) physics is then broached [54–61]. The physics of high harmonic generation has been the subject of recent reviews [45, 52].

An important feature of high harmonic light for use in applications is that the intensity of the harmonics exhibits a plateau, such that the number of photons created in these harmonics is roughly constant over a wide range of photon energy. For example, the intensity of harmonics 21–101 generated from a Ti:sapphire laser operating at 806 nm can vary by less than one order of magnitude [62].

The principle of operation of this source is conceptionally simple, as shown in figure 1. The output of the Ti:sapphire laser is focused into a gas, most commonly a rare gas, contained in a cell, a capillary or a molecular beam. If the laser power density is of the order of 10^{14} W cm^{-2} (plus or minus one order of magnitude), harmonic generation ensues [63]. In the plateau region, conversion efficiencies as high as 10^{-6} are routinely obtained [64]. This can be improved upon with phase-matched harmonic generation [61, 65–68]. An efficiency of as high as 10^{-5} in the 40–70 eV range was demonstrated by Murnane, Kapteyn and co-workers [65] and this group [61, 66–69] along with those of Krausz and co-workers [51–53, 59, 70, 71] and L'Huillier, Wahlström and co-workers [54, 60, 63, 72–75] have continued to push for higher efficiencies and shorter wavelengths. Continuous tunability is afforded by tuning either the fundamental or second harmonic (generated in a BBO crystal) of the Ti:sapphire laser itself. The Ti:sapphire laser commonly operates at a repetition rate of 1 kHz.

In most configurations, the harmonics are dispersed by a monochrometer. The wavelength resolution is not determined by the grating but by the laser pulse. This has the advantage over a broadband source such as a synchrotron of minimizing the intensity loss due to monochromatization since entrance and exit slits need not be used. However, the monochrometer introduces significant group velocity dispersion, which stretches the pulses temporally out of the attosecond and into the femtosecond or even picosecond regime. Compression with a second grating, while feasible, would entail a prohibitive loss of photons. An alternative, though expensive, scheme for separating the harmonics involves the use of multilayer mirrors. These mirrors can be made to pass a single harmonic and do not introduce pulse stretching [76]. The downside is that each harmonic requires a mirror designed

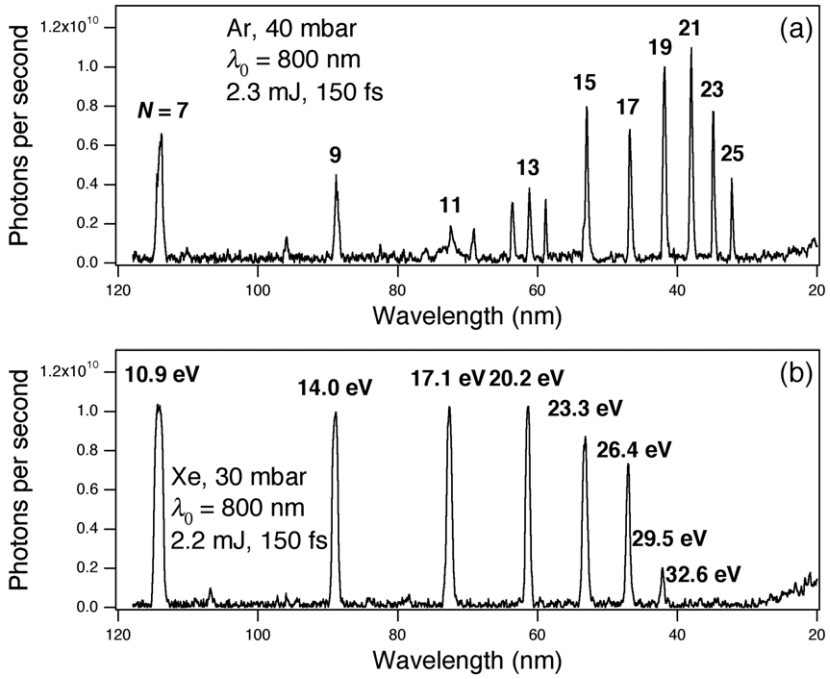

Figure 2. Spectra of high harmonics produced by the interaction of 150 fs pulses from a Ti:sapphire laser with (a) Ar and (b) Xe. The focusing and gas pressure conditions were chosen to enhance intensity near the cutoff region for Ar whereas the flatness of the plateau region was optimized in the Xe spectrum.

specifically for its wavelength and angle of incidence. Note further that the attosecond scale structure *within* a pulse requires the bandwidth of a number of harmonics and that this structure is lost in any scheme that spectrally resolves the harmonics [54–61, 77].

The highest harmonic order $N_{\max}$ that can be reached in a nonphase-matched geometry is given by

$$N_{\max} = \frac{I_p + 3.17U_p}{h\nu}, \tag{2}$$

where $h\nu = 1.55$ eV is the photon energy of the laser fundamental (here taken to be a Ti:sapphire laser operating at 800 nm) and I_p is the ionization potential of the gas. When performed in a waveguide to limit plasma-induced laser beam defocusing, this cutoff can be substantially extended [68]. U_p is the ponderomotive energy, which denotes the energy that the free electron can acquire in the laser field after the tunnelling process, and is given by [73]

$$U_p = \frac{E^2}{4\omega^2}. \tag{3}$$

In equation (3), E is the electric field amplitude (V cm^{-1}) and ω is the laser frequency. The spectrum of harmonics has the general shape shown in figure 2. The $N = 3$ and 5 peaks exhibit relatively high conversion efficiency that can be described by perturbation theories. Round about $N = 7$ or 9, the plateau region settles into a rather flat intensity distribution that extends to $N_{\max}$.

Figure 2 also demonstrates two other important characteristics. For a given laser system, the cutoff is determined by the ionization potential of the gas, whereas the intensity scales

with the polarizability of the gas. Thus Xe exhibits the highest conversion efficiency but lowest energy cutoff. Using He as the plasma gas leads to lower conversion efficiencies but a significantly higher energy cutoff. The cutoff for Xe found in figure 2 is $N_{max} = 19$ (∼29.5 eV), while that for Ar is $N_{max} = 25$ (∼41.9 eV). The flatness of the plateau depends on experimental parameters such as the gas pressure and the focusing geometry. Intensities of $\sim 10^6$–10^7 photons per pulse were produced in the plateau region, after the selection by the grating. With a 1 kHz repetition rate this corresponds to $\sim 10^{10}$ photons s^{-1}.

A typical system for the implementation of HHG in surface science, such as those used in the groups of Kolasinski and Palmer [78–80], Heinzmann [76], Zacharias [81, 82], and Kapteyn and Murnane [83], can be split in four sections: (i) the laser system, (ii) the interaction region for HHG, (iii) the harmonics separation chamber, and (iv) the surface science UHV chamber, as shown in figure 1.

The most common laser system for producing the fundamental radiation is a mode-locked Ti:sapphire laser delivering several mJ pulses into ∼100 fs or shorter pulses at ∼800 nm. Significant advantages in boosting conversion efficiency can be had by reducing pulse widths to 30 fs or less and by using a long confocal parameter focusing geometry. The restriction of a long confocal parameter essentially means that it is much more favourable to push the laser fluence to the required 10^{14} W cm^{-2} by using higher pulse energy and shorter pulses rather than focusing more tightly. Fluences much above 10^{15} W cm^{-2} are counterproductive because ionization becomes too facile and coherence is not easily maintained over a wide range of photon energies in the highly ionized plasma. In this case, HHG only occurs on the rising edge of the pump pulse before the maximum intensity is reached unless the pulse is kept significantly shorter than 100 fs. Short pulses are also essential for extending the energy range of HHG. Emission at the 297th harmonic (2.7 nm) has been observed [50] and it has been shown [51, 71] that sub-10 fs pulses are critical to the generation of light in the water window (2.3–4.4 nm), a region of great interest for the probing of biological tissues.

The interaction region poses the following conundrum:

(i) we are attempting to confine a high pressure gas (several to several hundred mbar) exclusively to a pathlength corresponding to the coherence length of the optical interaction (essentially the several centimetres of the confocal parameter or length of the capillary),
(ii) while an entrance window is possible, the exit side must be able to withstand a pressure gradient, high power IR irradiation and pass the wavelengths of interest,
(iii) the pressure must drop rapidly outside of the interaction region and in the wavelength separation chamber so as to avoid reabsorption, and
(iv) we have to get rid of the vast majority of the fundamental IR light.

The use of molecular beams and capillaries can reduce the pumping requirements substantially. A pinhole aperture or thin (∼100 nm) Al window can be used to separate the interaction region from the harmonics separation chamber. The filter allows for a usable photon energy range of 14–72 eV with a nearly constant transmittance of 80% [84]. Alternatively, a beamsplitter composed of Si or SiC plates and set at the Brewster angle can be used [85]. The reflectivity is a function of wavelength but has been shown to be 56% at 29.6 nm. Sufficient baffling is required to suppress scattered IR.

The harmonics are separated in a differentially pumped chamber containing either a toroidal grating or multilayer mirrors. The design specifications of the separation element determine the throughput and spectral range that can be addressed and there is generally a trade off between the breadth of the spectral range that can be covered and the transmission loss. The separation element is also chosen to be a focusing optic so that the harmonics are

separated and focused with a minimum of surface interactions and loss. Because of the wide range of photon energies, astigmatism can be a serious problem.

3. Applications of high harmonic generation to surface science

As a result of the short penetration depth of VUV and XUV light, an HHG source can be used to probe the optical and electronic properties of thin films. Several studies have been performed along these lines and are reviewed here, whereas those involving photochemistry are dealt with in the next section.

Riedel *et al* [78] probed the fluorescence decay of sodium salicylate ($C_7H_5NaO_3$) and the polymer poly(ethylene)terephthalate (PET, $(C_{10}H_8O_4)_n$). The former is conventionally used as a scintillator. The latter is a polymer studied in electroluminescence for potential use as an OLED (organic light emitting diode) [86]. Both emit strong luminescence, after excitation, from the first excited singlet state at 3.04 eV (∼410 nm) and 3.6 eV (∼344 nm) for sodium salicylate and PET, respectively. Sodium salicylate exhibits a simple exponential decay corresponding to a lifetime of $t_1 = 8.8 \pm 0.4$ ns. The PET fluorescence decay is not composed of a single component and has been fitted by a combination of an exponential decay and a second nonlinear term describing a local density induced quenching (LDI quenching) process. LDI has previously been observed for NaI and CsI [87] when irradiated with heavy charged particles, and exhibits this type of non-exponential decay behaviour. In fact, the first part of the PET fluorescence decay for the short times ($t < 15$ ns) is linear and corresponds to the classical exponential decay of the first singlet excited state ($t_2 = 16.2$ ns $\pm$ 0.6 ns). The second part is characteristic of a delayed fluorescence due to nonlinear effects linked with the intensity applied to the polymer film. These phenomena can occur when the density of electrons in the conduction band is high enough to produce dipole–dipole interactions with localized excitons. Thus HHG generated XUV light can be used to engender a nonlinear phenomenon in the photoluminescent polymer PET.

The first application of HHG to surface science was the pioneering photoemission work of Haight and co-workers [88–93]. They investigated electron dynamics at the Ge(111):As surface as well as high resolution core level spectroscopy of GaAs(110), Pb and an In_2I_6 thin film. A normally unoccupied surface state on Ge(111):As was observed at 0.43 ± 0.04 eV above the Ge valence band maximum. This state is populated by photoexcited hot electrons, which relax by exchanging energy with lattice phonons over the first few tens of picoseconds. These electrons cool but mainly remain in the normally unoccupied state, which exhibits a radiative lifetime of the order of 200–500 ps.

Zacharias and co-workers used HHG to produce radiation in the range 11–60 eV to investigate polarization and angle resolved photoemission [84, 94, 95]. They investigated clean and c(4 × 2)-2CO-covered Pt(111) surfaces. They observed a previously unreported resonance in the CO photoemission spectrum that was attributed to electrons from the occupied 3σ level excited into the unoccupied 2π level followed by the autoionization of the 1π CO state or Auger decay. In the normal emission spectra of Pt(111), three peaks associated with Pt surface states at fixed kinetic energies of 10, 12.5 and 19 eV were observed. These normally unoccupied states were populated by inelastic scattering of the primary photoexcited electrons.

Heinzmann and co-workers have also investigated electron dynamics at surfaces with the use of HHG. They performed pump–probe measurements of the hot electron distribution created by a femtosecond pulse at 1.5 eV incident on Pt(110)-(1 × 2). The hot electrons were probed by an HHG pulse at 70 eV with a pulsewidth of ∼70 fs, which allowed them to follow the relaxation of electrons excited above the Fermi energy (E_F). In accord with previous measurements [96], electrons with an energy of ∼1.5 eV above E_F have a lifetime

near 10 fs. They have also examined charge carrier dynamics on semiconductor surfaces [97] by measuring the kinetic-energy shifts of Ga 3d core level photoelectrons after excitation with 3.1 eV femtosecond laser pulses. Carrier transport from the bulk to the surface was observed to occur within 500 fs after photoexcitation, while relaxation of the excited state populated in this way evolves on a timescale of a few tens of picoseconds. Drescher *et al* [98, 99] then proceeded to determine directly in the time domain with attosecond resolution the relaxation dynamics of core-excited atoms. They measured a lifetime of $7.9^{+1.0}_{-0.9}$ fs for M shell (3d orbital) vacancies of Kr using pump–probe techniques.

Shimizu *et al* [100] measured the temperature-dependent decay dynamics of innershell holes in CsBr with the aid of HHG. Lifetimes as short as 1.5 ps at 340 K were measured.

Murnane and co-workers have used photoemission induced by photons at the 27th HHG harmonic (42 eV) to monitor the changes that occur when O_2 chemisorbed on Pt(111) is excited by an 800 nm, 22 fs pulse [16, 17]. A low IR fluence of 1 mJ cm^{-2} was used to avoid photodesorption while exciting ∼6% of the surface electrons. The electron distribution is found to thermalize within <250 fs. A transient change in the O_2 $1\pi_g^*$ level occurs, which exhibits an onset time of 550 ± 140 fs but which decays in ∼5 ps. The occupation of this level is indicative of a transformation of chemisorbed O_2 from the superoxo (O_2^-) to the peroxo (O_2^{2-}) species. The transient change in the O_2 photoelectron spectrum is, therefore, likely due to the transient formation of a peroxo species.

4. Surface photochemistry in the VUV

Surface photochemical processes are general divided into two classes:

(i) *direct photoexcitation of the adsorbate*; with characteristics modified from those observed in the gas phase due to selective quenching of excited adsorbate states and to the post-dissociation interaction between the photochemical reaction products and the substrate; and

(ii) *substrate mediated processes*, which can be driven either by hot electrons (with energies above E_F but below the vacuum level E_V) or photoelectrons (in which the photoelectron flux induces electron-stimulated reactions analogous to those observed in electron scattering processes).

Hence, electron stimulated desorption (ESD) and photon stimulated desorption (PSD) can share common mechanistic elements. The commonalities shared in the chemistry induced by ionizing radiation has, of course, been recognized in other environments and is of great importance in the electron initiated chemistry of water and aqueous systems [101]. The presence of the substrate can also lead to a completely new channel that combines elements of both [102], in which electron attachment to a resonantly pumped, photoexcited molecular state occurs. This process has no gas or bulk condensed phase analogue. However, it is precisely the VUV region of the spectrum in which excited electronic states of the adsorbate are accessible by direct, resonant photon absorption.

While most of the attention is heaped on the electrons, it is important to remember that hot holes can also be responsible for driving surface photochemistry. For instance, Kolasinski [103] has shown that photoexcitation of a hydrogen-terminated silicon surface in an aqueous fluoride solution leads to an *increase by over ten orders of magnitude in the sticking coefficient* of F^-. This is the first step in the etching of the Si; hence, the rate of etching is increased by the same amount.

Desorption induced by electronic transitions (DIET) at energies corresponding to the VUV and XUV in the system of hydrogen adsorbed on silicon—whether induced by photons,

electrons or a scanning probe tip—has recently been reviewed by Kolasinski [104] and will not be reviewed here. This system exhibits DIET via a low-lying electronic state that can be excited with electrons from the tip of a scanning tunnelling microscope (STM). Recent experiments have demonstrated a correspondence to photodesorption because excitation of the same electronic state with photons from a F_2 laser can also lead to stimulated desorption. The F_2 laser, which operates at 7.9 eV (157 nm), will become increasingly commonly used. Much more will be done at this wavelength, not only because of the improvement in commercial lasers but also because this wavelength is being considered for commercial photolithographic applications.

In the next two sections, the VUV photochemistry of two very different molecular systems is reviewed. These two systems both exhibit very weak interactions with the graphite substrate; therefore, strong perturbations of the molecular response to VUV light should not be induced. The two systems exhibit very different lateral (adsorbate–adsorbate) interactions. In the case of water, hydrogen bonding is much stronger than the water–graphite interaction. It is also much stronger than the magnetic interactions that are responsible for the ordering of O_2/graphite multilayers. The resulting structures of the films also differ significantly. In figure 3, a hydrogen-bonded ice unit as well as the 4 ML O_2 structure are depicted. The ice structure attempts to maximize hydrogen bonding by pointing H atoms at neighbouring O atoms. In the O_2 structure, the molecules are aligned parallel to the surface normal.

4.1. H_2O

The chemistry induced by electronic excitation of water ices at energies corresponding to the vacuum ultraviolet (VUV) region is of particular interest in an astrochemical [3, 4, 105–117] as well as an atmospheric [118, 119] setting. The interaction of UV and VUV light with ice-covered dust grains is a potential source of many complex molecules that are observed in the interstellar medium [109]. Photochemistry and photodesorption are both important processes since photochemistry may lead to the production of new chemical species on the dust grains and photodesorption provides a pathway to expel these species into the interstellar gas phase, even though the surface temperature may well be below 10 K.

Baggott *et al* [120] performed surface photochemistry experiments on amorphous H_2O/D_2O ice adsorbed on highly oriented pyrolytic graphite (HOPG) at 80 K using a high intensity VUV helium lamp (VSI model UVS 300), which could deliver up to 2×10^{13} photons cm^{-2} s^{-1} with 21.21 eV (He I) and 40.82 eV (He II). Desorbed positive ions were detected during 500 s irradiation with a pulse counting quadrupole mass spectrometer (QMS) placed normal to the surface. Multiplexed mass spectra were recorded such that several masses could be simultaneously monitored.

D^+ and D_3O^+ (figure 4) are the predominant desorption products from a D_2O ice layer, whereas H^+ and H_3O^+ are the primary products from H_2O ice on graphite. While this may seem obvious, interesting observations include that the ratios of the desorption intensities for these pairs of ions depends on the photon energy, the coverage and the isotopomers excited. The molecular ions are only observed for 41 eV excitation, their relative rate of desorption is highest at low coverage and whereas more H^+ is formed than H_3O^+, more D_3O^+ is formed compared to D^+. Furthermore, no D_2O^+ is formed nor is the desorption of OD^+, O_2^+, DO_2^+ or $D_2O_2^+$ observed. The latter species would all be expected if photodissociation fragments were building up on the surface.

The water/graphite interaction is very weak and the binding energy of water is dominated by hydrogen bonding within the adsorbed layer. Therefore any perturbation of the water photochemistry is not related to the formation of covalent bonds with the surface. In

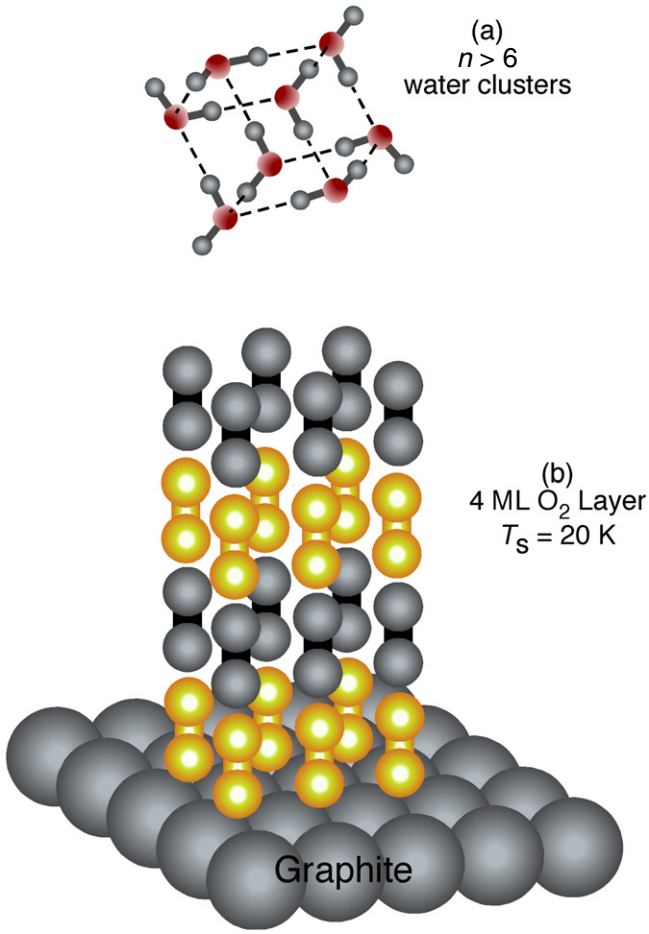

Figure 3. Depictions of the structures formed (a) when six or more water molecules cluster into cage-like structures and (b) when 4 ML of O_2 are dosed onto graphite at 20 K and align along the surface normal.

(This figure is in colour only in the electronic version)

small gas-phase clusters of H_2O, the low-lying electronic excitations are well localized on individual water molecules; nonetheless, the presence of hydrogen bonding appears to affect the photodissociation dynamics [121]. The influence of adsorption on a metal surface upon water ESD has been studied by Noell *et al* [122] who performed detailed studies of the yield and kinetic energy distribution of H^+ desorbed from H_2O adsorbed on Ni(111). The threshold for H^+ desorption was found at an incident energy of 20–21 eV. This is significantly above the gas-phase threshold for dissociative photoionization (DPI) of 18.76 eV, where a significant H^+ yield is observed. In this study, as well as earlier ESD [123] and photon stimulated desorption (PSD) [124] studies, Stulen and co-workers determined that H^+ was the majority cationic species being desorbed. This is consistent with a number of other DIET studies of adsorbed H_2O, both for ESD [125–127] and PSD [128, 129].

Orlando and co-workers have carried out extensive studies of desorption and chemistry induced by 5–250 eV electrons on water films adsorbed on Pt(111) [118, 119]. These studies

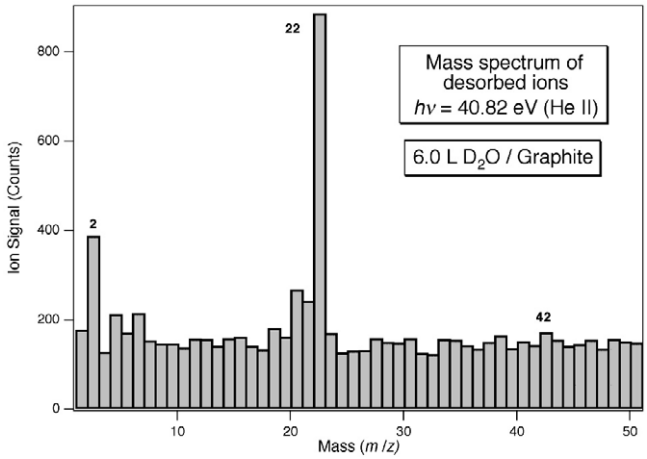

Figure 4. The mass spectrum of ions photodesorbed from a graphite surface which has been exposed to 6 L of D_2O at $T_s = 80$ K followed by irradiation with 40.82 eV photons.

are reviewed elsewhere. They observed two thresholds for D^+ desorption from adsorbed D_2O near 22–24 and ∼40 eV. The TOF distribution is at least bimodal, indicating multiple desorption channels. Two-hole, one-electron states are thought to be primarily responsible for excitations that lead to D^+ desorption. Photodissociation of H_2O and photodesorption of H atoms occurs at much lower photon energies. The photochemistry of thin water layers on Pd surfaces has been extensively studied by Hasselbrink and co-workers [130–132]. Yabushita *et al* [133] have measured the kinetic energy distributions of H atoms produced by 193 nm irradiation of thick H_2O films. They observed a distribution consisting of fast (0.39 eV) and thermalized (120 K, 0.02 eV) components.

Water is thought to form a mixture of 2D and 3D clusters on a graphite surface [134]. Because of the weak interaction with the surface, adsorbed water clusters probably have structures close to those found in the gas phase [135–138] consistent with recent calculations by Cabrera Sanfelix *et al* [139] and Lin *et al* [140]. The structure and dynamics of protonated [141–144] and anionic [144] water clusters has been the subject of much recent interest. Small gas-phase water clusters ($n < 7$) form 2D ring structures. Larger clusters form 3D cubic structures; however, numerous isomers have similar energies. Small 2D water clusters such as those known in the gas phase have a co-ordination number of just two. Surface water molecules in the perfect bulk structure have a co-ordination number of three and some expose free OD bonds that point along the surface normal [145]. As the coverage increases the proportion of 3D clusters increases and the average co-ordination number of water increases towards its bulk value of ∼4. Thus, as the coverage increases, there is an increase in the mean co-ordination number.

In the gas phase, excitation at both 21 and 41 eV leads to dissociative photoionization, which results in D^+ production. The nascent photochemically produced D^+ can

(i) leave the adsorbed cluster directly if it is produced on a free OD bond;
(ii) scatter off of a neighbouring D_2O to which it is hydrogen bonded and then leave the surface after an inelastic collision;
(iii) scatter off a neighbouring D_2O, recombine with it and leave as D_3O^+; or
(iv) scatter off a neighbour and be retained by the cluster.

Process (iii) is a type of surface aligned photochemistry [146]. Reactions similar to the ion–molecule reaction that leads to the creation of D_3O^+ have been observed for photon or electron-driven dissociation at surfaces for several other neutral–neutral [147–154] and ion–molecule [118, 119, 155–157] systems. The kinetic energy of photochemically produced H atoms and probability for it to undergo these types of processes has recently been treated theoretically for much lower excitation energies [158].

The threshold D^+ kinetic energy required to rip the desorbing D_3O^+ from the surface is provided by the kinetic energy of the photochemically produced D^+. This energy when zero, one, two, three or four hydrogen bonds are broken is estimated to be 6.6, 9.4, 12.1, 14.9 and 17.6 eV, respectively. Consequentially, desorbed D_3O^+ is most likely to be formed from D_2O that is adsorbed in low co-ordination sites. In extended ice films (>50 ML thick) the formation of $H^+(H_2O)_n$ cluster ions is also very sensitive to the film structure, the extent of hydrogen bonding and the presence of defects [118, 119]. Cluster formation from extended films predominantly appears at a threshold energy of 70 eV and is thought to be initiated by the localization of a two-hole state and Coulomb repulsion between the molecular ion and the second hole.

The H^+ kinetic energy distributions measured by Noell *et al* [122] in ESD from H_2O films at an incident energy of 45 eV extends beyond 10 eV. At 21 eV incident energy, however, the desorbed H^+ has a distribution that is substantially less energetic, peaking below 1 eV. Assuming that the same excited states are involved in ESD and PSD, the kinetic energy distributions measured by Noell *et al* should be similar to those that pertain to the experiment of Baggott *et al* and explains why no D_3O^+ is produced at 21 eV excitation. The liberated D^+ simply does not have sufficient energy to form and then dislodge D_3O^+ from the surface (even in the absence of hydrogen bonding). For 41 eV excitation, a substantial fraction of the D^+ does have sufficient energy to form and dislodge D_3O^+ from low co-ordination sites. However, since the mean co-ordination number increases with increasing coverage, the relative D_3O^+ yield drops with increasing coverage. This momentum transfer model of D_3O^+ production is supported further by considering that the H^+:H_3O^+ signal ratio is >1, whereas the D^+:D_3O^+ signal ratio is <1. Since H^+ is lighter than D^+, it must have significantly more initial kinetic energy to impart enough momentum to form and dislodge H_3O^+ from the surface.

Using a simple statistical argument based on the relative coverages of free and hydrogen-bonded OD moieties, *if* hydrogen-bonded and free O–D bonds undergo DPI *with equal probability*, the D^+:D_3O^+ desorption ratio should *not be less than 1:1* at low coverage and should *decrease* with increasing coverage. Neither of these predictions is corroborated by the data. To explain why the D_3O^+ signal exceeds the D^+ signal and why the D^+:D_3O^+ ratio changes as it does with increasing coverage, Baggott *et al* speculated that there is a propensity for the hydrogen-bonded O–D to break preferentially over the free O–D bond. The barrier into the more exothermic $D_3O^+ + OD$ channel is lower than the barrier into the less exothermic $D^+ + OD$ channel, which leads to preferential photodissociation of the hydrogen-bonded O–D bond compared to the free O–D bonds.

4.2. O_2

The dynamics of the electronic states of the free O_2 molecule are well known from gas-phase studies [159–162] and comparisons with the adsorbed phase lead to insights into the effects of adsorption on electronic structure and dynamics. It is also of interest to compare the VUV photochemistry of physisorbed O_2 to that of chemisorbed O_2, such as O_2 chemisorbed on Si(111)-(7 × 7) [13]. Previous synchrotron-based studies [102, 163–165] of physisorbed O_2 on graphite have revealed interesting dynamics that appear to be operative only at higher photon energies.

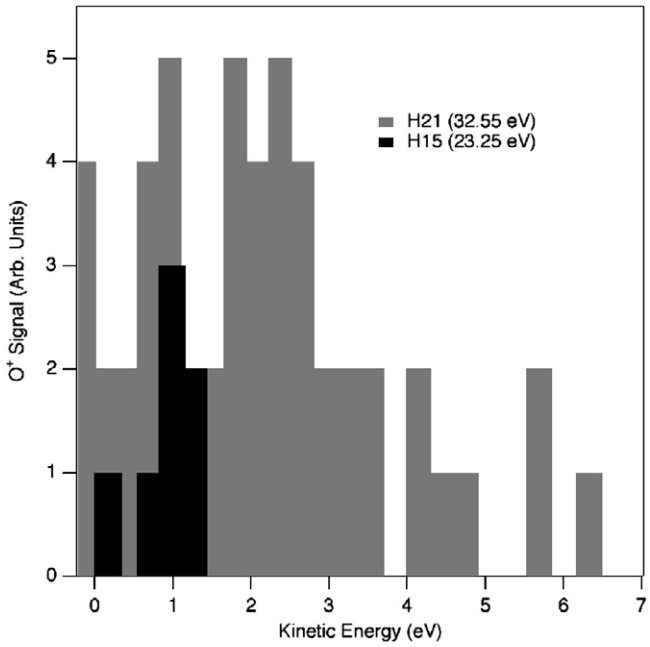

Figure 5. Time-of flight spectrum recorded for O^+ photodesorbed from a 4 ML physisorbed layer of O_2/graphite for VUV light produced by HHG for photon energies below (23.25 eV) and above (32.55 eV) the threshold for a rapidly increasing photodesorption cross section.

Riedel *et al* [15] used HHG generated light (10–38 eV, harmonics 7–23), to induce photodesorption of O^+ from the dissociative photoionization of O_2/graphite. The physisorbed O_2 assumes the 4 ML structure depicted in figure 3(b). The pulsed nature of the HHG source was used to facilitate time-of-flight (TOF) measurements of the desorbed O^+ kinetic energy.

O^+ was the only species observed to desorb. It exhibits a threshold at a photon energy of ∼17 eV. The cross section for desorption increases substantially above 29 eV. As shown in figure 5, the kinetic energy distribution of desorbed O^+ changes substantially above and below the 29 eV threshold. The increased desorption threshold corresponds to the opening of channels that release high kinetic energy O^+ from the surface. Comparison to the kinetic energy distributions observed in the gas phase reveals that the high-energy side of the distributions is little changed between the adsorbed phase and the gas phase. The low energy side, however, is drastically transformed by adsorption. In the gas phase, the predominant pathway for DPI leads to low energy O^+ for both 21 and 41 eV irradiation. This channel is shut down in the DPI of physisorbed O_2. Whereas the excitation step appears to be little influenced by the presence of the substrate and neighbouring O_2 molecules, the departure dynamics are significantly different when comparing gas-phase DPI and adsorbed-phase DPI. In the adsorbed phase, the departing O^+, even though it points along the surface normal, must overcome the image potential it experiences due to the surface. Zero kinetic energy and slow O^+ ions will be captured by the image potential and cannot desorb. On the basis of energetics and the similarity of the DPI kinetic energy distributions, the photodesorption of O^+ is assigned to a direct rather than a substrate mediated process.

The VUV photochemistry of O_2 adsorbed on a polycrystalline Pt [166] or Si surface [13] was investigated by Dujardin *et al*. Both O^+ and O^- were observed to desorb from multilayers

of O_2 physisorbed on Pt for irradiation with $\geqslant$17 eV photons, with a strong increase above 32 eV. O_2^+ and O_2^- were also observed but with much lower probabilities. The interaction of photoelectrons with adsorbed O_2 was shown to be responsible for dissociative desorption. Resonant structure in the desorption yield was ascribed to photoionization of adsorbed O_2, which produced photoelectrons that go on to interact with neighbouring O_2 molecules. The molecular ions result from post-dissociation interaction of O^+ or O^- with neighbouring molecules. Note that for this system, *no alignment* of the O_2 along the surface normal has been observed and, therefore, geometric consideration leads to enhanced post-dissociation interactions compared to the O_2/graphite system.

On Si(111)-(7 $\times$ 7), O_2 chemisorbs with its molecular axis *parallel* to the surface. Synchrotron radiation of 10–150 eV was used to study the desorption of O^+ from these layers [13]. A threshold energy for desorption of O^+ is found at 33 eV, significantly higher than in the physisorbed systems, and was assigned to the direct excitation of the $2\sigma_g$ electron of chemisorbed O_2. A second threshold at 100 eV along with resonances in the O^+ desorption yield were observed at 108 and 115 eV. The 100 eV threshold corresponds to a Si(2p) excitation. The 108 eV resonance corresponds to the interaction of the Si(2p) photoelectron with the $O_2(3\sigma_u)$ level located 8 eV above E_F. The second resonance may correspond to a multiple electron excitation and the assignment remains unclear. The kinetic energy distribution of O^+ desorbed by 46 eV photons exhibits one broad peak at 2.5 eV rather than the two peaks at 1 and 2.1 eV observed from O_2/graphite. For photodesorption at 108 eV on O_2/Si, a second high energy peak at 9 eV is observed.

5. Concluding remarks

The VUV and XUV are extremely rich regions of the electromagnetic spectrum in which to study surface photochemistry and electron dynamics. Surface photochemistry and electron dynamics are linked both by the relaxations of excited electronic states and by the importance of electron/adsorbate scattering in photochemistry. There have been great advances in the past two decades in the sources of photons in these spectral regions and these advances have brought us incredibly powerful probes of dynamical phenomena with unprecedented abilities to study temporally resolved behaviour with high energy resolution. More importantly, these sources also now deliver useful quantities of photons. The progress of high harmonic generation has been particularly impressive as it has evolved from a curiosity in high field physics, to a tabletop light source that can routinely deliver intense VUV and XUV light.

Several examples of the utilization of HHG in surface experiments pertaining to photoemission, photoluminescence and photochemistry have been reviewed and demonstrate that this technique is a highly useful source of photons for the study of dynamics. The VUV and XUX photochemistry of two very different molecular systems, which interact weakly with a graphite substrate but which exhibit either strong hydrogen bonding (H_2O) or weak magnetic interactions (O_2), has been discussed. The lateral interactions lead to very different adsorbate layer structures and the products of the photochemical reactions reflect these differences.

In water clusters, dissociative photoionization leads to the direct desorption of H^+ as well as the formation and desorption of H_3O^+ via an ion–molecule reaction. The strong lateral interactions in water clusters lead to significant differences between the photochemistry of isolated water and condensed water. Whereas high kinetic energy H^+ can be formed in either case, obviously, the formation H_3O^+ can only occur when the dissociating molecule has an immediate neighbour. More importantly, it appears that the hydrogen bonding present in the cluster leads to preferential breakage of a hydrogen-bonded O–H compared to a free O–H bond.

Dissociative photoionization in multilayer O_2 films, in which the molecular axis is pointed along the surface normal, leads exclusively to the formation of O^+. In this case, the dissociative ionization process is little perturbed by the presence of neighbouring O_2 molecules and the proximity of the graphite substrate. One significant difference, however, is noted. In the gas phase, the predominant pathways lead to a maximum probability of forming O^+ at near zero kinetic energy. In surface dissociative photoionization, these pathways are not able to result in photodesorption because the image potential of the ion leads to trapping before desorption. The photodesorption probability, therefore, is biased toward high kinetic energy channels. When the molecular axis is directed away from the surface normal as in O_2 physisorbed on Pt, then the molecular ions O_2^+ and O_2^- were also observed due to interactions that occur after the initial dissociation event.

Acknowledgments

I wish to thank my co-workers who helped make these studies possible: Simeon Baggott, John Foord, Richard Palmer, Luís Perdigão, Luis Hernández Pozos, and Damien Riedel. Funding was provided by the Engineering and Physical Sciences Research Council (UK) and the European Union's TMR program. This work was supported by the University of Virginia and the National Science Foundation IGERT program under grant #9972790.

References

[1] Samson J A R 1967 *Techniques of Vacuum Ultraviolet Spectroscopy* (New York: Wiley)
[2] Kunz C (ed) 1979 *Synchrotron Radiation: Techniques and Applications* (*Springer Topics in Current Physics* vol 10) (Berlin: Springer)
[3] Ruffle D P and Herbst E 2000 *Mon. Not. R. Astron. Soc.* **322** 770
[4] Willacy K and Langer W D 2000 *Astrophys. J.* **544** 903
[5] Madey T E, Johnson R E and Orlando T M 2002 *Surf. Sci.* **500** 838
[6] Wallraff G M and Hinsberg W D 1999 *Chem. Rev.* **99** 1801
[7] Chapman H N *et al* 2001 *J. Vac. Sci. Technol.* B **19** 2389
[8] Gwyn C W, Stulen R, Sweeney D and Attwood D 1998 *J. Vac. Sci. Technol.* B **16** 3142
[9] Banine V and Moors R 2004 *J. Phys. D: Appl. Phys.* **37** 3207
[10] Stamm U 2004 *J. Phys. D: Appl. Phys.* **37** 3244
[11] Mendes P M and Preece J A 2004 *Curr. Opin. Colloids Interface Sci.* **9** 236
[12] Petravic M, Deenapanray P N K, Comtet G, Hellner L, Dujardin G and Usher B F 2000 *Phys. Rev. Lett.* **84** 2255
[13] Dujardin G, Comtet G, Hellner L, Hirayama T, Rose M, Philippe L and Besnardramage M J 1994 *Phys. Rev. Lett.* **73** 1727
[14] Hatano Y 1999 *Phys. Rep.* **313** 110
[15] Riedel D, Perdigão L M A, Hernández-Pozos J L, Guo Q, Palmer R E, Foord J S and Kolasinski K W 2002 *Phys. Rev.* B **66** 233405
[16] Bauer M, Lei C, Read K, Tobey R, Gland J, Murnane M M and Kapteyn H C 2001 *Phys. Rev. Lett.* **87** 025501
[17] Lei C, Bauer M, Read K, Tobey R, Liu Y, Popmintchev T, Murnane M M and Kapteyn H C 2002 *Phys. Rev.* B **66** 245420
[18] Warwick T, Arthur J, Padmore H A and Stöhr J (ed) 2004 *Synchrotron Radiation Instrumentation* (*AIP Conf. Proc.* vol 705) (Melville, NY: American Institute of Physics)
[19] Lipson R H, Dimov S S, Wang P, Shi Y J, Mao D M, Hu X K and Vanstone J 2000 *Instrum. Sci. Technol.* **28** 85
[20] Couprie M-E and Ortéga J-M 2000 *Analysis* **28** 725
[21] O'Shea P G and Freund H P 2001 *Science* **292** 1853
[22] Feldhaus J, Arthur J and Hastings J B 2005 *J. Phys. B: At. Mol. Opt. Phys.* **38** S799
[23] Anderson S L, Kubiak G D and Zare R N 1984 *Chem. Phys. Lett.* **105** 22
[24] Kubiak G D, Sitz G O and Zare R N 1984 *J. Chem. Phys.* **81** 6397
[25] Kolasinski K W, Shane S F and Zare R N 1992 *J. Chem. Phys.* **96** 3995
[26] Kolasinski K W 1995 *Int. J. Mod. Phys.* B **9** 2753

[27] Bent S F, Michelsen H A and Zare R N 1995 *Laser Spectroscopy and Photochemistry on Metal Surfaces* ed H L Dai and W Ho (Singapore: World Scientific) p 977
[28] Michelsen H A, Rettner C T and Auerbach D J 1994 *Surface Reactions* (*Springer Series in Surface Sciences* vol 34) ed R J Madix (Berlin: Springer) p 185
[29] Woodruff D P (ed) 2003 *The Chemical Physics of Solid Surfaces: Surface Dynamics* vol 11 (Amsterdam: Elsevier)
[30] Hodgson R T, Sorokin P P and Wynne J J 1974 *Phys. Rev. Lett.* **32** 343
[31] Brunner T A 2003 *J. Vac. Sci. Technol.* B **21** 2632
[32] Hansson B A M and Hertz H M 2004 *J. Phys. D: Appl. Phys.* **37** 3233
[33] Hector S 2005 *Solid State Technol.* (March) Online, O1
[34] Turcu I C E and Dance J B 1999 *X-rays from Laser Plasmas: Generation and Applications* (Chichester: Wiley)
[35] Janulewicz K A, Lucianetti A, Priebe G and Nickles P V 2004 *X-ray Spectrom.* **33** 262
[36] Matthews D L *et al* 1985 *Phys. Rev. Lett.* **54** 110
[37] Rosen M D *et al* 1985 *Phys. Rev. Lett.* **54** 106
[38] Suckewer S, Skinner C H, Milchberg H, Keane C and Voorhees D 1985 *Phys. Rev. Lett.* **55** 1753
[39] Rocca J J 1999 *Rev. Sci. Instrum.* **70** 3799
[40] Lemoff B E, Barty C P J and Harris S E 1994 *Opt. Lett.* **19** 569
[41] Moses E I and Weust C R 2005 *Fusion Sci. Technol.* **47** 314
[42] Danson C N *et al* 2005 *Laser Particle Beams* **23** 87
[43] Zeitoun P *et al* 2004 *Nature* **431** 426
[44] Corkum P B 1993 *Phys. Rev. Lett.* **71** 1994
[45] Eden J G 2004 *Prog. Quantum Electron.* **28** 197
[46] Hay N, Castillejo M, de Nalda R, Springate E, Mendham K J and Marangos J P 2000 *Phys. Rev.* A **61** 053810
[47] Lyngå C, L'Huillier A and Wahlström C G 1996 *J. Phys. B: At. Mol. Opt. Phys.* **29** 3293
[48] Fraser D J, Hutchinson M H R, Marangos J P, Shao Y L, Tisch J W G and Castillejo M 1995 *J. Phys. B: At. Mol. Opt. Phys.* **28** L739
[49] Liang Y, Augst S, Chin S L, Beaudoin Y and Chaker M 1994 *J. Phys. B: At. Mol. Opt. Phys.* **27** 5119
[50] Chang Z, Rundquist A, Wang H, Murnane M M and Kapteyn H C 1997 *Phys. Rev. Lett.* **79** 2967
[51] Spielmann C, Burnett N H, Sartania S, Koppitsch R, Schnürer M, Kan C, Lenzner M, Wobrauschek P and Krausz F 1997 *Science* **278** 661
[52] Brabec T and Krausz F 2000 *Rev. Mod. Phys.* **72** 545
[53] Seres E, Seres J, Krausz F and Spielmann C 2004 *Phys. Rev. Lett.* **92** 163002
[54] Antoine P, L'Huillier A and Lewenstein M 1996 *Phys. Rev. Lett.* **77** 1234
[55] Papadogiannis N A, Vitzel B, Kalpouzos C and Charalambidis D 1999 *Phys. Rev. Lett.* **83** 4289
[56] Christov I P 1999 *Phys. Rev.* A **60** 3244
[57] Scrinzi A, Geissler M and Brabec T 2001 *Phys. Rev. Lett.* **86** 412
[58] Paul P M, Toma E S, Breger P, Mullot G, Augé F, Balcou P, Muller H G and Agostini P 2001 *Science* **292** 1689
[59] Drescher M, Hentschel M, Kienberger R, Tempea G, Spielmann C, Reider G A, Corkum P B and Krausz F 2001 *Science* **291** 1923
[60] López-Martens R *et al* 2005 *Phys. Rev. Lett.* **94** 033001
[61] Kapteyn H C, Murnane M M and Christov I P 2005 *Phys. Today* **58** 39
[62] Macklin J J, Kmetec J D and Gordon C L III 1993 *Phys. Rev. Lett.* **70** 766
[63] L'Huillier A, Lompré L-A, Mainfray G and Manus C 1992 *Advances in Atomic, Molecular, and Optical Physics: Supplement 1. Atoms in Intense Laser Fields* ed M Gavrila (Boston, MA: Academic) p 139
[64] L'Huillier A and Balcou P 1993 *Phys. Rev. Lett.* **70** 774
[65] Rundquist A, Durfee C G III, Chang Z, Herne C, Backus S, Murnane M M and Kapteyn H C 1998 *Science* **280** 1412
[66] Gibson E A *et al* 2003 *Science* **302** 95
[67] Paul A, Bartels R A, Tobey R, Green H, Weiman S, Christov I P, Murnane M M, Kapteyn H C and Backus S 2003 *Nature* **421** 51
[68] Gibson E A, Paul A, Wagner N, Tobey R, Backus S, Christov I P, Murnane M M and Kapteyn H C 2004 *Phys. Rev. Lett.* **92** 033001
[69] Bartels R, Backus S, Zeek E, Misoguti L, Vdovin G, Christov I P, Murnane M M and Kapteyn H C 2000 *Nature* **406** 164
[70] Apolonski A, Poppe A, Tempea G, Spielmann C, Udem T, Hozwarth R, Hänsch T W and Krausz F 2000 *Phys. Rev. Lett.* **85** 740
[71] Schnürer M, Streli C, Wobrauschek P, Hentschel M, Kienberger R, Spielmann C and Krausz F 2000 *Phys. Rev. Lett.* **85** 3392

[72] L'Huillier A, Schafer K J and Kulander K C 1991 *Phys. Rev. Lett.* **66** 2200
[73] Wahlström C G 1994 *Phys. Scr.* **49** 201
[74] Mercer I, Mevel E, Zerne R, L'Huillier A, Antoine P and Wahlström C-G 1996 *Phys. Rev. Lett.* **77** 1731
[75] Bellini M, Lyngå C, Tozzi A, Gaarde M B, Hänsch T W, L'Huillier A and Wahlström C-G 1998 *Phys. Rev. Lett.* **81** 297
[76] Siffalovic P, Drescher M, Spieweck M, Wiesenthal T, Lim Y C, Weidner R, Elizarov A and Heinzmann U 2001 *Rev. Sci. Instrum.* **72** 30
[77] Corkum P B, Burnett N H and Ivanov M Y 1994 *Opt. Lett.* **19** 1870
[78] Riedel D, Hernández-Pozos J L, Baggott S, Kolasinski K W, Palmer R E and Foord J S 2001 *Rev. Sci. Instrum.* **72** 1977
[79] Riedel D, Hernández-Pozos J L, Kolasinski K W, Baggott S and Palmer R E 2001 *J. Physique* IV **11** 73
[80] Riedel D, Hernández-Pozos L, Baggott S, Kolasinski K W and Palmer R E 2001 *J. Physique* IV **11** 499
[81] Kutzner J, Silies M, Witting T, Tsilimis G and Zacharias H 2004 *Appl. Phys.* A **78** 949
[82] Hagedorn M, Kutzner J, Tsilimis G and Zacharias H 2003 *Appl. Phys.* A **77** 49
[83] Bauer M, Lei C, Tobey R, Murnane M M and Kapteyn H 2003 *Surf. Sci.* **532–535** 1159
[84] Tsilimis G, Kutzner J and Zacharias H 2003 *Surf. Sci.* **528** 171
[85] Takahashi E J, Hasegawa H, Nabekawa Y and Midorikawa K 2004 *Opt. Lett.* **29** 507
[86] Mary D, Albertini M and Laurent C 1997 *J. Phys. D: Appl. Phys.* **30** 171
[87] Belsky A N, Glukhov R A, Kamenskikh I A, Martin P, Mikhailin V V, Munro I H P C, Shaw D A, Shpinkov I N and Vasilev A N 1996 *J. Electron Spectrosc. Relat. Phenom.* **79** 147
[88] Haight R and Peale D R 1993 *Phys. Rev. Lett.* **70** 3979
[89] Haight R and Peale D R 1994 *Rev. Sci. Instrum.* **65** 1853
[90] Haight R 1995 *Surf. Sci. Rep.* **21** 275
[91] Haight R and Seidler P F 1994 *Appl. Phys. Lett.* **65** 517
[92] Rettenberger A and Haight R 1998 *Surf. Sci.* **414** 197
[93] Haight R 1996 *Chem. Phys.* **205** 231
[94] Tsilimis G, Kutzner J and Zacharias H 2003 *Appl. Phys.* A **76** 743
[95] Tsilimis G, Fecher G H, Braun J, Kutzner J and Zacharias H 2004 *Appl. Phys.* A **78** 177
[96] Fann W S, Storz R, Tom H W K and Bokor J 1992 *Phys. Rev. Lett.* **68** 2834
[97] Siffalovic P, Drescher M and Heinzmann U 2002 *Europhys. Lett.* **60** 924
[98] Drescher M, Hentschel M, Kienberger R, Uiberacker M, Yakovlev V, Scrinizi A, Westerwalbesloh T, Kleineberg U, Heinzmann U and Krausz F 2002 *Nature* **419** 803
[99] Drescher M, Hentschel M, Kienberger R, Uiberacker M, Westerwalbesloh T, Kleineberg U, Heinzmann U and Krausz F 2004 *J. Electron Spectrosc. Relat. Phenom.* **137** 259
[100] Shimizu T, Sekikawa T, Kanai T, Watanabe S and Itoh M 2003 *Phys. Rev. Lett.* **91** 017401
[101] Garrett B C *et al* 2005 *Chem. Rev.* **105** 355
[102] Šiller L, Bennett S L, MacDonald M A, Bennett R A, Palmer R E and Foord J S 1996 *Phys. Rev. Lett.* **76** 1960
[103] Kolasinski K W 2003 *Phys. Chem. Chem. Phys.* **5** 1270
[104] Kolasinski K W 2004 *Curr. Opin. Solid State Mater. Sci.* **8** 353
[105] Wu C Y R, Yang B W and Judge D L 1994 *Planet. Space Sci.* **42** 273
[106] Shi M, Baragiola R A, Grosjean D E, Johnson R E, Jurac S and Schou J 1995 *J. Geophys. Res. Planets* **100** 26387
[107] Westley M S, Baragiola R A, Johnson R E and Baratta G A 1995 *Planet. Space Sci.* **43** 1311
[108] Westley M S, Baragiola R A, Johnson R E and Baratta G A 1995 *Nature* **375** 405
[109] Gerakines P A, Schutte W A and Ehrenfreund P 1996 *Astron. Astrophys.* **312** 289
[110] Frank L A, Paterson W R, Ackerson K L and Bolton S J 1997 *Geophys. Res. Lett.* **24** 2151
[111] Johnson R E and Quickenden T I 1997 *J. Geophys. Res. Planets* **102** 10985
[112] Sieger M T, Simpson W C and Orlando T M 1998 *Nature* **394** 554
[113] Watanabe N, Horii T and Kouchi A 2000 *Astrophys. J.* **541** 772
[114] Manicò G, Ragunì G, Pirronello V, Roser J E and Vidali G 2001 *Astrophys. J.* **548** L253
[115] Fraser H J, Collings M P and McCoustra M R S 2002 *Rev. Sci. Instrum.* **73** 2161
[116] Baragiola R A 2003 *Planet. Space Sci.* **51** 953
[117] Leto G and Baratta G A 2003 *Astron. Astrophys.* **397** 7
[118] Herring-Captain J, Grieves G A, Alexandrov A, Sieger M T, Chen H and Orlando T M 2005 *Phys. Rev.* B **72** 035431
[119] Herring J, Alexandrov A and Orlando T M 2004 *Phys. Rev. Lett.* **92** 187602
[120] Baggott S R, Kolasinski K W, Perdigão L M A, Guo Q and Palmer R E 2002 *J. Chem. Phys.* **117** 6667
[121] Chipman D M 2005 *J. Chem. Phys.* **122** 044111

[122] Noell J O, Melius C F and Stulen R H 1985 *Surf. Sci.* **157** 119
[123] Stulen R H 1983 *J. Vac. Sci. Technol.* A **1** 1163
[124] Rosenberg R A, Rehn V, Jones V O, Green A K, Parks C C, Loubriel G and Stulen R H 1981 *Chem. Phys. Lett.* **80** 488
[125] Madey T E and Yates J T Jr 1977 *Chem. Phys. Lett.* **51** 77
[126] Stulen R H and Thiel P A 1985 *Surf. Sci.* **157** 99
[127] Bennett S L, Greenwood C L, Williams E M and Segovia J L 1991 *Surf. Sci.* **251/252** 857
[128] Stockbauer R, Hanson D M, Flodström S A and Madey T E 1982 *Phys. Rev.* B **26** 1885
[129] Kurtz R L, Stockbauer R, Madey T E, Román E and De Segovia J L 1989 *Surf. Sci.* **218** 178
[130] Zhu X-Y, White J M, Wolf M, Hasselbrink E and Ertl G 1991 *J. Phys. Chem.* **95** 8393
[131] Wolf M, Nettesheim S, White J M, Hasselbrink E and Ertl G 1991 *J. Chem. Phys.* **94** 4609
[132] Wolf M, Nettesheim S, White J M, Hasselbrink E and Ertl G 1990 *J. Chem. Phys.* **92** 1509
[133] Yabushita A, Hashikawa Y, Ikeda A, Kawasaki M and Tachikawa H 2004 *J. Chem. Phys.* **120** 5463
[134] Chakarov D V, Österlund L and Kasemo B 1995 *Langmuir* **11** 1201
[135] Mejías J A and Lago S 2000 *J. Chem. Phys.* **113** 7306
[136] Day P N, Pachter R, Gordon M S and Merrill G N 2000 *J. Chem. Phys.* **112** 2063
[137] Miller Y, Fredj E, Harvey J N and Gerber R B 2004 *J. Phys. Chem.* A **108** 4405
[138] Diri K, Myshakin E M and Jordan K D 2005 *J. Phys. Chem.* A **109** 4005
[139] Cabrera Sanfelix P, Holloway S, Kolasinski K W and Darling G R 2003 *Surf. Sci.* **532–535** 166
[140] Lin C S, Zhang R Q, Lee S T, Elstner M, Frauenheim T and Wan L J 2005 *J. Phys. Chem.* B **109** 14183
[141] Christie R A and Jordan K D 2002 *J. Phys. Chem.* B **106** 8376
[142] Shin J W, Hammer N I, Diken E G, Johnson M A, Walters R S, Jaeger T D, Duncan M A, Christie R A and Jordan K D 2004 *Science* **304** 1137
[143] Headrick J M, Diken E G, Walters R S, Hammer N I, Christie R A, Cui J, Myshakin E M, Duncan M A, Johnson M A and Jordan K D 2005 *Science* **308** 1765
[144] Jordan K D 2004 *Science* **306** 618
[145] Materer N, Starke U, Barbieri A, Van Hove M A, Somorjai G A, Kroes G J and Minot C 1997 *Surf. Sci.* **381** 190
[146] Polanyi J C and Williams R J 1988 *J. Chem. Phys.* **88** 3363
[147] Bourdon E B D, Das P, Harrison I, Polanyi J C, Segner J, Stanners C D, Williams R J and Young P A 1986 *Faraday Discuss.* **82** 343
[148] Mieher W D and Ho W 1989 *J. Chem. Phys.* **91** 2755
[149] Mieher W D and Ho W 1993 *J. Chem. Phys.* **99** 9279
[150] Deliwala S, Finlay R J, Goldman J R, Her T H, Mieher W D and Mazur E 1995 *Chem. Phys. Lett.* **242** 617
[151] Orlando T M, Burns A R, Stechel E B and Jennison D R 1990 *J. Chem. Phys.* **93** 9197
[152] Kimmel G A, Tonkyn R G and Orlando T M 1995 *Nucl. Instrum. Methods Phys. Res.* B **101** 179
[153] Kimmel G A and Orlando T M 1996 *Phys. Rev. Lett.* **77** 3983
[154] Kimmel G A and Orlando T M 1995 *Phys. Rev. Lett.* **75** 2606
[155] Goldby I M, Guest R J and Palmer R E 1993 *Chem. Phys. Lett.* **206** 181
[156] Šiller L, Hedhili M N, Le Coat Y, Azria R and Tronc M 1999 *J. Chem. Phys.* **110** 10554
[157] Lee J-G, Hong S-H, Ahner J and Yates J T Jr 2002 *Phys. Rev. Lett.* **89** 235202
[158] Andersson S, Kroes G J and van Dishoeck E F 2005 *Chem. Phys. Lett.* **408** 415
[159] Gardner J L and Samson J A R 1975 *J. Chem. Phys.* **62** 4460
[160] Akahori T, Morioka Y, Watanabe M, Hayaishi T, Ito K and Nakamura M 1985 *J. Phys. B: At. Mol. Phys.* **18** 2219
[161] Lafosse A, Brenot J C, Golovin A V, Guyon P M, Hoejrup K, Houver J C, Lebech M and Dowek D 2001 *J. Chem. Phys.* **114** 6605
[162] Lu Y, He Z X, Cutler J N, Southworth S H, Stolte W C and Samson J A R 1998 *J. Electron Spectrosc. Relat. Phenom.* **94** 135
[163] Bennett R A, Bennett S L, Šiller L, MacDonald M A, Palmer R E, Wright H M and Foord J S 1994 *J. Phys.: Condens. Matter* **6** 1955
[164] Šiller L, Bennett S L, Crabtree H M, Bennett R A, Wilkes J, Lamont C L A, MacDonald M A, Palmer R E and Foord J S 1997 *J. Phys.: Condens. Matter* **9** 5815
[165] Friedrich C M, Wilkes J, Palmer R E, Bennett S L, MacDonald M A, Lamont C L A and Foord J S 1995 *Chem. Phys. Lett.* **247** 348
[166] Dujardin G, Hellner L, Philippe L, Azria R and Besnardramage M J 1991 *Phys. Rev. Lett.* **67** 1844